RADIATION LEVELS AT THE LHC: 2012, 2015 AND 2016 PROTON PHYSICS OPERATIONS IN VIEW OF HL-LHC REQUIREMENTS

C. Martinella†, M. Brugger, S. Danzeca, R. Garcia Alia,
Y. Kadi, O. Stein, C. Xu, CERN Switzerland
University of Jyväskylä, Jyväskylä, Finland

Abstract

The variety of beam losses produced in the Large Hadron Collider (LHC) creates a mixed and complex radiation field. During 2012, 2015 and 2016, Beam Loss Monitors and RadMons were used to monitor the integrated dose and the High Energy Hadrons fluence in order to anticipate the electronics degradation and investigate the cause of failures. The annual radiation levels are compared; highlighting the mechanisms in the production of beam losses and the impact of the different squeeze and crossing angle. In addition, the increase of beam-gas interaction is discussed comparing operations at 25 ns and 50 ns bunch spacing. A strategy is presented to allow for a continuous respective evaluation during the upcoming LHC and future High Luminosity LHC (HL-LHC) operations.

INTRODUCTION

During the LHC operation beam losses occur and create a mixed and complex radiation environment that can induce a significant risk for the electronic systems which are not specifically designed to be radiation tolerant. This includes the risk of Single Event Effects (SEE) with a possible direct impact on beam operation. Also the long-term cumulative effect needs to be considered. In order to reduce the number of failures and maximize the operation of the equipment, it is important to monitor and determine the expected radiation levels in these areas.

In the LHC the sources of losses relevant for radiation effects in electronics are produced according to three main mechanisms; particle debris generated from the experiments, beam losses in absorbers and collimators and beam-gas interactions inside the beam pipe around the entire ring. The radiation field varies significantly in terms of particle type and energy for the different areas. Usually two locations are used as reference for LHC; the tunnel and the shielded areas. In this paper the attention will focus in the tunnel areas where the electronic equipment, located on the floor below the beam line, can potentially be exposed to High Energy Hadron (>20 MeV) fluences of 10^{11} [HEH/cm^2 year] and energies up to 100 GeV [1].

The RadMon System allows the continuous measurement of the quantities important for radiation effects on the electronics. A total of 380 RadMons are installed in the tunnel and in the shielded areas of LHC. Here commercial SRAM memories are used to measure the HEH and the thermal neutron fluence by counting the Single Event Upsets (SEU) [2]. For low statistics, below 10^8 HEH/cm^2 year (corresponding to ~50 SEU counts), the relative error is above 40% (e.g. in the arcs). However for higher counts the error is dominated by the spread and the uncertainty over the thermal neutron contribution. In this case, a relative error of 25% is normally considered.

To optimize the coverage of the electronic equipment a new schema for the RadMon locations in the Dispersion Suppressors (areas between the arcs and long straight sections) was implemented during the 2016 winter technical stop and will be complemented with Monte Carlo FLUKA simulations, also for the HL-LHC scenario.

In addition, almost 3900 ionization chambers (50 cm long filled with N_2 at 100 mbar overpressure, sensitive volume of 1.5 liter) are installed around the ring to measure the secondary shower outside the cryostat. The aim of the Beam Loss Monitoring System (BLM) is to protect the superconducting magnets from the quenching by generating a beam dump when the detected losses exceed certain thresholds. Furthermore, by measuring the loss pattern, the BLM system enables the identification of loss mechanisms in the LHC [3].

During the 2012, 2015 and 2016 proton operations several dumps were attributed to the electronic failures induced by radiation (see Table 1). The number of dumps per unit luminosity [dump / fb^{-1}] in 2015 and 2016 were significantly lower than in 2012. This was mainly due to the implemented R2E (Radiation to Electronics) mitigation measures such as improvements on the quench protection or powering electronics.

Table 1: Number of Dump per Integrated Luminosity

Year	2012	2015	2016
Dump/Lum.	3 /fb^{-1}	1.2 /fb^{-1}	0.15 /fb^{-1}

To minimize the future downtime of the accelerator caused by failures induced by radiation, a detailed knowledge of the radiation field and beam loss productions in LHC is required to allow predictions for the HL-LHC operations.

For this reason, the measurements performed during the different years are used as a baseline to scale the radiation levels. Several parameters have to be considered for the scaling, such as the proportionality between the intensity and the luminosity through the beam optics (e.g. crossing angle, beta-star), the increase of energy, the collimator settings and the residual gas density of the vacuum in the beam pipes around the entire ring.

† corinna.martinella@cern.ch

ISBN 978-3-95450-182-3

Copyright © 2017 CC-BY-3.0 and by the respective authors

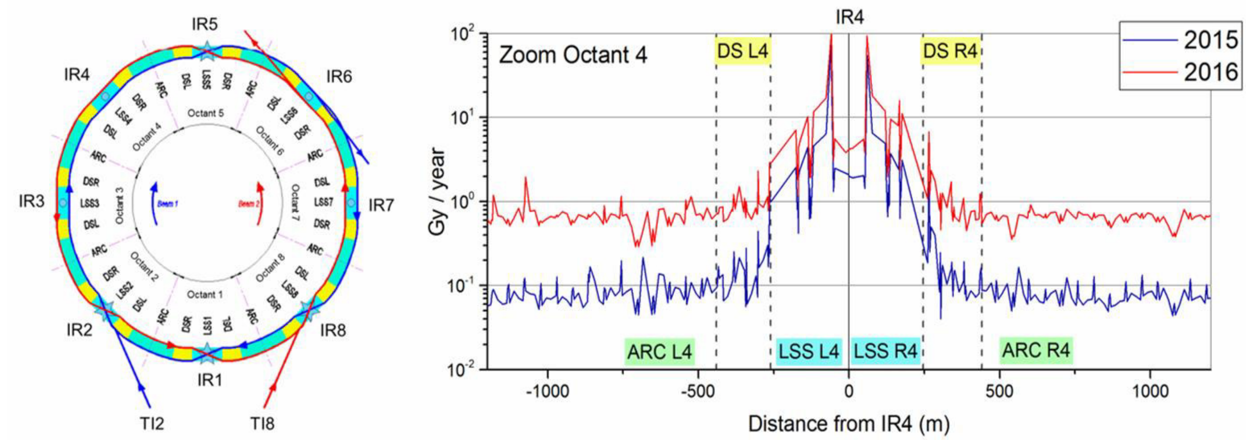

Figure 1: Layout of the LHC (left). Zoom of the annual doses measured with the BLM in the octant 4 (right). Long straight sections (LSS), dispersion suppressors (DS) and arcs (ARC) are highlighted for the left (L) and right (R) sides.

EVOLUTION OF RADIATION LEVELS DURING THE PROTON RUN

Layout

The LHC is 26.7 km long. The ring is divided in 8 octants. Each octants starts from the middle of an arc and finishes at the middle of the following arc, it contains 34 left and 34 right cells (see Figure 1). There are 8 Long Straight Sections (LSS: cell 1-7 left and righ). The exact layout depends on the specific use of the insertion, e.g. beam collisions for physics (IR1, IR2, IR5, IR8), beam dumping (IR6), beam cleaning (IR3, IR7) or RF system (IR4).
16 Dispersion Suppressor (DS: cell 8-11) help in matching the insertion optics of the Long Straight Section to the periodic solution of the arc (ARC: cell 12-34).

General overview

2015 was a re-commissioning and re-conditioning year. The LHC restarted after the Long Shutdown (LS1) and the run was dedicated to the exploration of operation at 6.5 TeV per beam and 25 ns bunch spacing. At the end of the run 4.2 fb^{-1} were recorded for ATLAS and CMS.
The full year of exploitation of LHC at the beam energy of 6.5 TeV was in 2016. Compared to 2015 the beam sizes at the high-luminosity interaction points were smaller and the crossing angle was reduced. For this reason, as visible in Table 2, the ratio between the total intensity integrated over the fills and the luminosity decreased by a factor 2.5 for 2016. This resulted in a proton-proton luminosity delivery to ATLAS and CMS 40% above the design value. The final integrated luminosity averaged 40.8 fb^{-1} in ATLAS/CMS, 1.8 fb^{-1} to LHCb and 13.4 pb^{-1} to ALICE.

Table 2: Integrated Luminosity in ATLAS and CMS (fb^{-1}), Integrated Intensity (proton x second) and Ratio (ps/fb^{-1})

Year	Lum	Intensity	Int/Lum
2015	4.2 fb^{-1}	6.46E+20 ps	1.5E+20(ps/fb^{-1})
2016	40.8 fb^{-1}	2.47E+21 ps	6.0E+19(ps/fb^{-1})

The following sections are focused on the loss mechanisms in the most critical areas.

High luminosity insertions: IR1 and IR5

Close to the high luminosity experiments, ATLAS and CMS, the particle debris generated from the collisions are the dominant effect in the production of losses. In Figure 2, the impact of the luminosity is shown for IR1 on top (ATLAS) and IR5 on bottom (CMS).
The ratio of the measurements between 2015 and 2016 is normalized both with the total intensity integrated over the fills (protons x second) and the accumulated luminosity (fb^{-1}). In the Long Straight Sections (LSS), normalizing with the accumulated luminosity, the baseline values are closer to ~1 than with the intensity.
This is caused by the different proportionality between the intensity and the luminosity during 2015 and 2016 (impact of the squeeze and the crossing angle). Therefore, for the high luminosity insertions, the scaling improves with the accumulated luminosity.

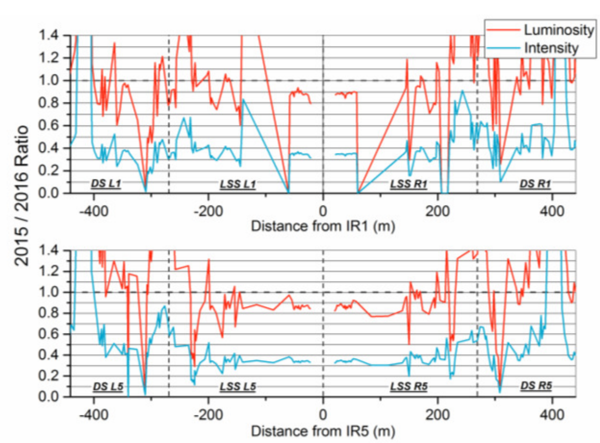

Figure 2: Ratio of BLM doses for 2015 and 2016 normalized with accumulated luminosity (fb-1) and integrated intensity (protons x seconds) for IR1 (top) and IR5 (bottom).

Copyright © 2017 CC-BY-3.0 and by the respective authors

More spikes are visible moving from the interaction regions. Here the luminosity scaling can be applied, but the contributions of the optics and the collimators settings need to be included and analysed to further refine the scaling.

Beam cleaning insertions: IR3 and IR7

Equivalent analysis of BLM measurements was done for IR3 and IR7 (see Figure 3), where the momentum cleaning and the betatron cleaning system are housed. In these regions, instead, the dominant effect is the production of losses during the beams collimation. Therefore the losses are proportional to the number of particles circulating. For this reason the scaling with the total integrated intensity improves with respect to luminosity, especially in high loss regions (baseline closer to ~1). To refine the scaling other parameters should be taken into considerations (e.g. fill lifetime and collimator settings).

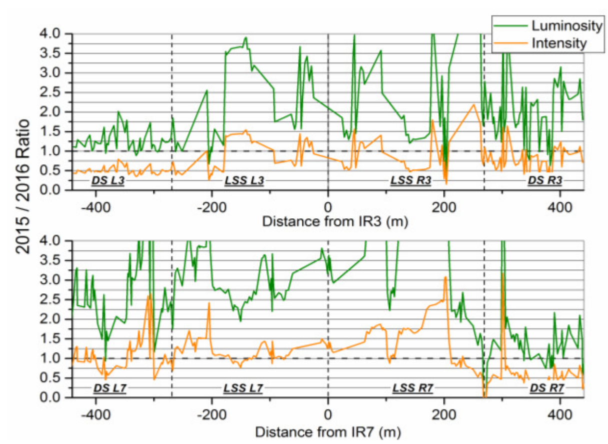

Figure 3: Ratio of BLM doses for 2015 and 2016 normalized with accumulated luminosity (fb^{-1}) and integrated intensity (protons x seconds) for IR3 (top) and IR7 (bottom).

ARCs

In the ARCs, since the losses are created from the beam-gas interaction, the radiation levels are proportional to the total circulating intensity of the beam (protons x second) and to the vacuum level.

The ratio of the HEH fluences measured with RadMon for the different years is shown in Figure 4 as function of the different cells in the DS and in the ARC. Only the right side of the octants is represented.

On top is the comparison between Run 1 (2012) and Run 2 (2016). The increase of the radiation levels was caused by the enlargement of the electron cloud effect moving from 50 ns bunch spacing operation (Run 1) to 25 ns in Run 2 and by the increase of beam energy from 4 TeV to 6.5 TeV. The middle graph shows the comparison between 2015 (run at 25 ns) and 2016. The baseline above the unit indicates higher fluences during 2015. This result can be attributed to a lower residual gas density due to a lower vacuum pressure during 2016 run. However this could not be confirmed through direct vacuum level measurements due to the sensitivity limitation of the vacuum gauges.

Finally, close to the high luminosity experiment (R1 and R5), in cell 9, 11, 13 and 15, the losses are caused by the dispersion function of the beam. Here the proportionality is with the luminosity, indeed the HEH fluences were higher during 2016. This is confirmed looking at the RadMon in cell 11 (DS) (bottom graph of Figure 4). Focusing on a single fill the HEH fluence is measured from the stable beam phase when the collisions begin in the experiments and the luminosity starts to be accumulated.

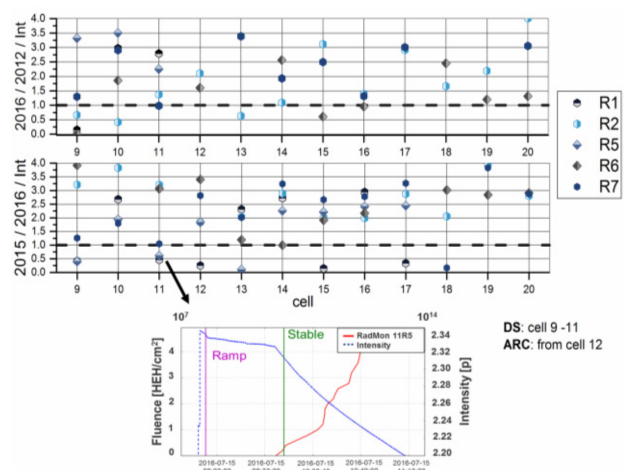

Figure 4: Ratio of annual HEH fluences from RadMon measurements (top and middle). HEH fluence measured from the RadMon in cell 11 during the fill 5096 (bottom).

CONCLUSION

During 2015 and 2016 the different squeeze and crossing angle impacted the proportionality between the integrated intensity and the accumulated luminosity. Comparing RadMon and BLM measurements the proportionality with the luminosity was identified for the high luminosity experimental regions (IR1 and IR5).

For the beam cleaning insertions (IR3 and IR7), the scaling improves with the intensity compared to luminosity, but additional factors such as the fill lifetime and the collimator settings need to be further investigated.

In the arcs the proportionality is with the circulating beam intensity, except for some peaks in the odd cells of the experimental points. Here, due to the dispersion function of the beams, the radiation levels are proportional to the luminosity. The vacuum pressure and the impact of the e-cloud effect needs to be considered as well for future operations.

REFERENCES

[1] K. Røed *et al.*, "Method for Measuring Mixed Field Radiation Levels Relevant for SEEs at the LHC", *IEEE Trans. Nucl. Sci., vol 59, no 4, August 2012.*

[2] G. Spiezia *et al.*, "The LHC Radiation Monitoring System – Radmon," *PoS, vol. RD11, p. 024, 2011.*

[3] E.B. Holzer *et al.*, "COMMISSIONING AND OPTIMIZATION OF THE LHC BLM SYSTEM", *Proceedings of HB2010, Morschach, Switzerland, 2010.*

Copyright © 2017 CC-BY-3.0 and by the respective authors

ISBN 978-3-95450-182-3